Aerosol Science and Technology

ISSN: 0278-6826 (Print) 1521-7388 (Online) Journal homepage: http://www.tandfonline.com/loi/uast20

Development of portable aerosol mobility spectrometer for personal and mobile aerosol measurement

Pramod Kulkarni, Chaolong Qi & Nobuhiko Fukushima

To cite this article: Pramod Kulkarni, Chaolong Qi & Nobuhiko Fukushima (2016) Development of portable aerosol mobility spectrometer for personal and mobile aerosol measurement, Aerosol Science and Technology, 50:11, 1167-1179, DOI: 10.1080/02786826.2016.1230662

To link to this article: http://dx.doi.org/10.1080/02786826.2016.1230662

AEROSOL SCIENCE AND TECHNOLOGY
2016, VOL. 50, NO. 11, 1167–1179
http://dx.doi.org/10.1080/02786826.2016.1230662

Taylor & Francis
Taylor & Francis Group

NEW GENERATION OF AEROSOL INSTRUMENTATION FOR DISTRIBUTED OR PERSONAL SAMPLING

Development of portable aerosol mobility spectrometer for personal and mobile aerosol measurement

Pramod Kulkarni[a], Chaolong Qi[a], and Nobuhiko Fukushima[b]

[a]Centers for Disease Control and Prevention, National Institute for Occupational Safety and Health Cincinnati, Ohio, USA; [b]Kanomax Japan Inc., Osaka, Japan

ABSTRACT

We describe development of a portable aerosol mobility spectrometer (PAMS) for size distribution measurement of submicrometer aerosol. The spectrometer is designed for use in personal or mobile aerosol characterization studies and measures approximately 22.5×22.5×15 cm and weighs about 4.5 kg including the battery. PAMS uses electrical mobility technique to measure number-weighted particle size distribution of aerosol in the 10–855 nm range. Aerosol particles are electrically charged using a dual-corona bipolar corona charger, followed by classification in a cylindrical miniature differential mobility analyzer. A condensation particle counter is used to detect and count particles. The mobility classifier was operated at an aerosol flow rate of 0.05 L/min, and at two different user-selectable sheath flows of 0.2 L/min (for wider size range 15–855 nm) and 0.4 L/min (for higher size resolution over the size range of 10.6–436 nm). The instrument was operated in voltage stepping mode to retrieve the size distribution in approximately 1–2 min. Sizing accuracy and resolution were probed and found to be within the 25% limit of NIOSH criterion for direct-reading instruments. Comparison of size distribution measurements from PAMS and other commercial mobility spectrometers showed good agreement. The instrument offers unique measurement capability for on-person or mobile size distribution measurement of ultrafine and nanoparticle aerosol.

ARTICLE HISTORY
Received 26 April 2016
Accepted 19 August 2016

EDITOR
Jingkun Jiang

1. Introduction

Recent growth in broad applications of nanotechnology has led to increase in industrial production of engineered nanomaterials. This has raised concerns over the potential risks to the human health from exposure to nanomaterials (NIOSH 2013). Recent field studies show that workers may be exposed to airborne engineered nanomaterials during the manufacturing, handling, and cleanup of carbon nanotube (CNT) materials (Birch et al. 2011; Dahm et al. 2012).

Depending on the nature of exposure, near real-time aerosol instruments can be useful in identifying sources, processes, or tasks that contribute to the release of nanomaterials in industrial environments (Methner et al. 2010). Several direct-reading instruments are available for workplace aerosol monitoring, which include hand-held condensation particle counters (CPCs), photometers, surface area monitors, scanning mobility particle sizers, and electrical impactors (Methner et al. 2010; Ramachandran et al. 2011; NIOSH 2013). The compact, hand-held instruments are suitable for routine use; however can only provide measurement of single metric such as number, surface area, or mass concentration. On the other hand, larger mobility spectrometers provide number-weighted particle size distribution, which can be used to obtain an estimation of all three exposure metrics in a single measurement. However, these instruments are not suitable for routine field use due to high cost, large weight, or complexity of use. In addition, these spectrometers use a radioactive source to achieve bipolar charge conditioning of the aerosol sample, which can restrict their transportation and field use. Other field-portable instruments, such as the Nano-ID (Particle Measuring Systems, Boulder, CO, USA), NanoScan (TSI Inc., Shoreview, MN, USA), and a hand-held particle size spectrometer (Qi and Kulkarni 2012) have been developed to measure the mobility size distribution. These instruments use a unipolar charger for charge-

CONTACT Pramod Kulkarni PSKulkarni@cdc.gov Centers for Disease Control and Prevention, National Institute for Occupational Safety and Health, 4676 Columbia Parkway, Cincinnati, OH 45226, USA.

Color versions of one or more of the figures in the article can be found online at www.tandfonline.com/uast.

Supplemental data for this article can be accessed on the publisher's website.

conditioning, which can introduce large measurement uncertainties for aerosols with preexisting charges (Qi et al. 2009 and limit the measurement size range (Qi and Kulkarni 2012).

In this article, we describe development of a compact, hand-portable, battery-operated mobility spectrometer that is suitable for aerosol size distribution measurement for personal, mobile, or distributed sampling applications. We present the design, development, and laboratory characterization of the instrument prototype, along with some representative field measurement applications of the instrument.

2. Portable aerosol mobility spectrometer (PAMS)

The layout of the various components of the prototype instrument and the flow scheme is shown in Figure 1a. The key components include a miniature dual-corona bipolar charger, a differential mobility electrical classifier, and a condensation particle counter. The aerosol particles are first electrically charged by the bipolar charger, then classified according to their electrical mobility in the classifier, and subsequently counted downstream using the condensation particle counter (CPC). A cyclone separator, with an aerodynamic diameter cut of 1000 nm (at 50% efficiency; see Figure S1 in the online supplementary information (SI) for transmission efficiency curve) at a flow rate of 0.7 litter per minute (L/min), is used upstream of the bipolar charger to remove larger particles from the aerosol entering the instrument. Key design features of each component are briefly described below.

2.1. Dual corona bipolar charger

A corona-based bipolar charger, described in an earlier publication (Qi and Kulkarni 2013), was used to charge-condition the aerosol entering the mobility classifier. This dual-corona bipolar charger (DCBC) employs an aerosol flow cavity exposed to two corona ionizers producing ions of opposite polarity. Each corona ionizer houses two electrodes in parallel needle-mesh configuration and is operated at the same magnitude of corona current (Figure S2 in the SI). The overall external dimensions of the DCBC were approximately $1.6\times1.9\times1.9$ cm. Experimental measurement of detailed charge distribution of near-monodisperse particles of different diameter in the submicrometer size range showed that the charger is capable of producing well-defined, consistent bipolar charge distributions for flow rates up to 1.5 L/min and aerosol concentration up to 10^7 cm^{-3} (Qi and Kulkarni 2013). For particles with preexisting charge of +1, 0, and −1, the measured charge distributions agreed well with the theoretical distributions within the range of experimental and theoretical uncertainties. The transmission efficiency of the charger was measured to be 80% for 10 nm particles (at 0.3 L/min and 5 μA corona current) and increased with increasing diameter beyond this size.

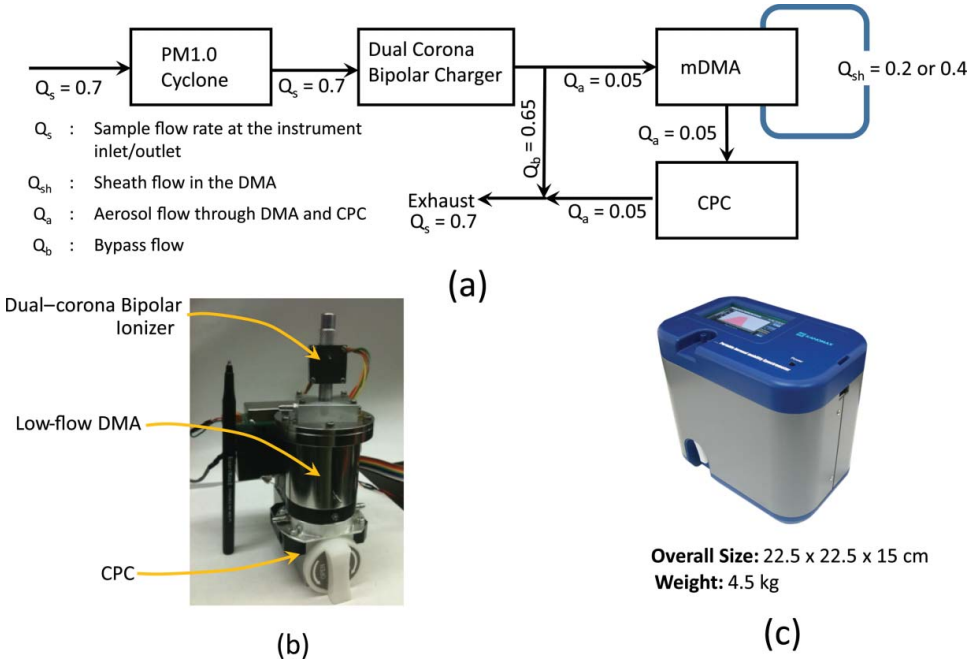

Figure 1. (a) Flow scheme and layout of different components of PAMS; (b) assembly of charger, DMA, and CPC units; (c) prototype PAMS instrument. Flow rates shown are in L/min.

Measurement of uncharged fractions at various combinations of positive and negative corona currents showed the charger performance to be insensitive to fluctuations in corona current. The *nt* product value (product of number concentration of ions *n*, and the residence time *t*) under positive corona operation was independently estimated to be 8.5×10^5 s/cm^3. The ion concentration estimates (Qi and Kulkarni 2013) indicate the charger to be capable of charge-conditioning typical atmospheric and industrial aerosols in most measurement applications. The miniature size, simple and robust operation makes the charger suitable for portable mobility spectrometers.

2.2. Miniature differential mobility classifier

A miniature differential mobility analyzer (mDMA) was designed for mobility classification. The details of the design and performance of this mDMA have been described elsewhere (Qi and Kulkarni 2016). Briefly, the mDMA was designed to allow classification of particle diameters up to 940 nm at an aerosol flow rate of ~0.05 L/min. The diameter of the inner cylindrical electrode was 1.778 cm. The inner diameter of the outer electrode was 2.54 cm (the distance between the electrodes was 3.81 mm). The length of electrodes from aerosol inlet and outlet in the classification region was 2.54 cm. The overall external dimensions of the mDMA were approximately 5.7×5.7×7.78 cm. The mDMA design was based on the theoretical breakdown strength of the electrical field of 43.5 kV/cm, which is marginally higher than that of the TSI 3081 and 3085 DMAs (43.1 kV/cm, TSI Inc., Shoreview, MN, USA). However, occasional breakdown was observed when exceeding voltage beyond 6.5 kV, which corresponds to a classified mobility diameter of 940 nm at a sheath flow rate of 0.2 L/min, and a breakdown strength of the electrical field of 20.5 kV/cm. Therefore, the upper limit of classifiable size was limited to 855 nm, with a maximum applied voltage of 5.8 kV. Some minor improvements to the design of the mDMA are expected to allow extension of the classification range to 1000 nm. The aerosol inlet was carefully designed to reduce diffusional loss of particles at low flow rates, and yet achieve uniform distribution in the azimuthal direction of the aerosol flow in the classification zone. Computational flow simulations were conducted to probe flow characteristics and velocity distribution in the classification region. Uniform circumferential flow distribution could be obtained at the design aerosol and sheath flow rates. This was also qualitatively confirmed with flow visualization using smoke, which revealed uniformly distributed (azimuthally) laminar flow (see Figure S3 in the SI). The transfer function of the DMA was characterized using tandem DMA (TDMA) experiments and found to agree well with the theoretical Stolzenburg transfer function (Stolzenburg 1988). The diffusional losses, represented by the reduction in the area under the transfer function curve, were found to be 84.45% at 10 nm, and reduced to 42.28% at 20 nm and 6.82% at 100 nm. These losses were lower than the losses in other DMAs operated at the same aerosol flow rate of 0.05 L/min, for instance, about 21.74% at 100 nm in Knutsen–Whitby long DMA (Stolzenburg 1988), and 10.37% at 100 nm in the Nano-DMA (Chen and Pui 1997). The voltage correction parameter, a fit parameter in the transfer function model (Qi and Kulkarni 2016), was determined experimentally and found to be close to 1.0 (average values were 1.015 and 0.953 at sheath flow rates of 0.2 and 0.4 L/min, respectively), and the broadening or dispersion of the transfer function could be adequately captured by particle's diffusivity at the 0.2 L/min sheath flow, requiring no further corrections. At a sheath flow rate of 0.4 L/min, a broadening correction factor of 1.3 was obtained from a least-square fitting process of all the experimental data at corresponding operating conditions. Experimentally measured and theoretical TDMA curves for 20 nm particles are shown in Figure S4 in the SI. The mobility uncertainty, based on the full width at half-max of the transfer function deconvoluted from the experimental TDMA curve, was approximately 34.2% at low resolution and 21.4% at high resolution for a 20 nm diameter particle. The finite mobility resolution of the DMA is likely the largest source of sizing uncertainty, since the other key sources of uncertainty, mainly from the variability in sheath flow, and voltage were estimated to be less than 3%. Uncertainty in charging characteristics could also affect sizing uncertainty; however these uncertainties are difficult to probe and were not investigated in this study. In addition to the sizing uncertainty, counting uncertainty also affects the overall uncertainty of size distribution measurement, which will be discussed later.

2.3. Condensation particle counter (CPC)

The CPC design was based on a conventional, laminar flow conductive cooling system employing isopropyl alcohol. The aerosol flow (0.05 L/min) was saturated using a porous tube at elevated temperature (40–50°C), which was subsequently cooled (to 10–20°C) to create a supersaturation. Temperature of both units was not actively controlled using a feedback loop (e.g., proportional–integral–derivative control) for simplicity; therefore, the temperatures could drift from desired values under extreme variations in ambient temperatures. However, these temperature excursions are not expected to be significant under typical temperature variations encountered in most workplaces. Under normal

operating conditions, the alcohol remains absorbed in the wick; however may seep out into the aerosol flow path by gravity if the azimuthal orientation of the prototype is excessively tilted. The residence time in the saturator and the condenser region was estimated to be 1.4 s each. The size of the grown droplet was estimated to be around 3–5 μm using Laser Doppler Velocimetry. At a given supersaturation ratio, the activation efficiency depends on the particle diameter, with efficiency decreasing with decreasing diameter. The activation efficiency of the CPC was experimentally determined using a reference Faraday-cage aerosol electrometer. At 25°C ambient temperature, the temperatures of the saturator and condenser were approximately 18 and 29°C. These temperatures varied slightly with the ambient temperature; however the temperature differential between and hot and cold sections (Δt) was constant at 11°C. Figure S5 in the SI shows the experimental setup used for measuring detection efficiency curve. Figure S6 in the SI shows detection efficiency of the CPC (η_{det}) as a function of particle diameter. The diameter of the particle activated with 50% efficiency (d_{50}) was estimated to be 7.5 nm. Since the temperatures of the saturator and condenser of the PAMS prototype were not actively controlled using a feedback loop, the temperature differential (Δt) drifted slightly with continuous operation of the instrument. After continuous operation over 1 h, the Δt decreased by 11%, which may lead to slight increase in d_{50}. This may lead to somewhat increased uncertainty of count measurement below <20 nm. These uncertainties can be minimized by implementing efficient temperature control of the CPC. Proper operation of the condensation particle counter also requires maintaining near-upright orientation.

2.4. Instrument operation

The instrument was operated at an inlet sample flow rate of 0.7 L/min. The flow through the inlet cyclone and DCBC was 0.7 L/min. The flow was split downstream of the charger to allow 0.05 L/min through the DMA and the CPC. The flow through the CPC was controlled by a critical orifice upstream of a pump and a solenoid valve on the excess/bypass flow line. The sheath flow in the DMA was provided by a miniature rotary vane pump operating in a closed loop. The sheath flow rate was controlled using a feedback from a flow meter. The temperature of the sheath flow was not actively controlled. The instrument was operated at two sheath flow rates, 0.2 and 0.4 L/min. The smaller sheath flow (0.2 L/min) allowed measurements over a wider size range from 15 to 855 nm, though at lower mobility resolution; whereas, the higher sheath flow rate was useful to obtain relatively higher resolution spectra in the size range 10–436 nm. The lower particle size limit was based on the limitation imposed by (i) resolution of the DMA, (ii) increased uncertainties from the miniature high voltage power supply, and (iii) the bit resolution of the microprocessor used for analog–to-digital conversion. The key operating characteristics of the prototype are listed in Table 1.

All three components (i.e., charger, mDMA, and CPC), including the optical module of the CPC could be integrated into a volume less than 15 × 10 × 8 cm^3 (Figure 1b). All pumps and electronics were battery operated using an on-board Li-ion battery. Data acquisition, control, and recording was accomplished using an on-board microprocessor. A straightforward zeroth inversion could be achieved using an on-board microprocessor. An off-line inversion routine was used to obtain size distributions, accounting for multiple charge states of particles. The overall dimensions of the entire prototype were approximately 22.5×22.5×15 cm and it weighed about 4.5 kg including the battery (Figure 1c). The prototype was capable of continuous measurements over 4 h on a full battery charge.

2.5. Particle size distribution retrieval

The instrument was operated in sequential voltage stepping mode to obtain number-weighted mobility distribution. Predetermined mDMA voltages (V_i) were sequentially applied for a predetermined amount of time (t_{step}) to measure corresponding number concentration (N_i) by the CPC at each voltage step. Based on the mobility resolution, the number of steps (and therefore channels in PSD) were determined to be 14 for low-resolution, and 26 for high-resolution operation. The central diameter of each channel in two resolution modes is provided in Table S1 in the SI.

The array of voltage (V_i) and number concentration (N_i) were used to obtain the mobility size distribution using an inversion procedure explained below.

The concentration response N_i of the instrument to an applied mDMA voltage V_i for a given size distribution $n(\log d_p)$ entering the inlet of the instrument is given by

$$N(V_j) = \sum_{i=1}^{M} \int_0^{\infty} \eta_{\mathrm{tot}}(d_p)\Omega(V_j,\ i, d_p) f_{\mathrm{chg}} \times (i, d_p)\, n(\log d_p).\, \mathrm{dlog}\, d_p, \quad [1]$$

where $\eta_{\mathrm{tot}}(d_p)$ is the total size-dependent particle detection efficiency, which is a product of the transmission efficiency of the mDMA (η_{DMA}), activation efficiency of the CPC

Table 1. Key operating parameters of the prototype PAMS.

Sample inlet flow rate	0.7 L/min
Aerosol flow rate through charger	0.7 L/min
Aerosol flow rate through DMA and CPC	0.05 L/min (50 cm^3/min)
Sheath flow rate	0.2 L/min, or 0.4 L/min
Size range	10.6–435.7 nm (at 0.4 L/min) 15.1–855 nm (at 0.2 L/min)

(η_{det}), diffusional wall losses in the transport lines (η_{diff}), transmission efficiency of the inlet cyclone (η_{cycl}), and the transmission efficiency of the bipolar charger (η_{chg}). $\Omega\left(V_j,\ i, d_p\right)$ is the transfer function of the mDMA, which accounts for the probability of passing particle of size (d_p) with elementary electric charge i at a given voltage (V_j), and $f_{chg}\left(i, d_p\right)$ is the probability that a particle of diameter d_p will carry charge i when it enters the classification zone in the classifier. Wiedensohler's approximation (Wiedensohler 1988) was used to describe the steady-state charge distribution $f_{chg}\left(i, d_p\right)$ based on the published data on the charging characteristics of this charger (Qi and Kulkarni 2013). Stolzenburg's model (Stolzenburg 1988) was used, which accounted for broadening due to Brownian diffusion. The prototype could display, in real-time, particle size distribution retrieved via zeroth-order inversion (assuming single charge on the particle). A more accurate particle size distribution was retrieved off-line using multiple charge correction algorithm of Hoppel (1978), following the methodical implementation outlined by He and Dhaniyala (2013).

3. Performance characterization of the prototype

3.1. Monodisperse aerosols

The performance of the prototype was evaluated using a laboratory electrical mobility spectrometer (EMS) consisting of a ^{85}Kr bipolar charger, followed by a Knutson–Whitby DMA (Model 3081, TSI Inc., Shoreview, MN, USA) and a CPC (Model 3025, TSI Inc.). The detailed schematic of the experimental setup used for this work is shown in the SI (Figure S7). Both silver nanoparticles (smaller than 50 nm from a tube furnace) and ammonium sulfate particles (50 nm and larger from a pneumatic atomizer) were used in the experiment. The EMS was operated at an aerosol flow rate of 0.3 L/min and the same aerosol-to-sheath flow ratio (β) as that of the PAMS. The centroid diameters of the bins used at low and high resolution are shown in Table S1 in the SI. To retrieve the size distribution, the EMS was operated in sequential voltage stepping mode with similar channel diameters and number of channels to those used in PAMS, and an identical inversion routine was used for both instruments. Geometric mean diameter and standard deviations of measured distributions were compared from both EMS and PAMS for several DMA-classified near-monodisperse aerosols. Performance was tested for both neutral aerosol, as well as those with preexisting charge of +1 entering the instrument inlets by turning the Soft X-Ray neutralizer (Model 3087, TSI Inc.) on and off upstream of the PAMS and EMS. Tables 2a and b shows this comparison. The distributions measured with PAMS of near-monodisperse aerosol show good agreement in geometric mean diameter d_{pg} and the geometric standard deviation (σ_g), regardless of the preexisting charge, confirming that the DCBC is able to adequately condition the charge on the aerosol to a pseudo-steady-state distribution. Comparison of d_{pg} from PAMS and EMS with the diameter of the DMA-classified test aerosol entering each instrument (i.e., input diameter) is used to quantify the accuracy or bias of particle size measurement. Table 2 shows that the agreement in input diameter (d_{DMA}; the first column) and the d_{pg} measured with both instruments is within 20%. Figures S8a and b in the SI show the distribution of relative bias b (defined as $b = \frac{d_{pg} - d_{DMA}}{d_{pg}}$) is less than 10% at high resolution and 20% at low resolution. Figure 2 shows comparison of d_{pg} measured by PAMS and EMS. This comparison includes polydisperse aerosols with total number concentration (N_{tot}) below and above 10^3 cm^{-3}, as well as monodisperse test aerosol (classified from DMA). The test using polydisperse aerosol of various concentrations was carried out by replacing the first DMA and the Soft X-ray neutralizer in the setup shown in Figure S7 with an adjustable aerosol dilutor. Most diameters agree within 15% (dotted line around 1:1 line in Figure 2), except for the very dilute polydisperse aerosol with N_{tot} of ~500 cm^{-3}. For this dilute aerosol, the difference in measured d_{pg} was as large as 40%. As shown by two inset histograms, the d_{pg} for 73% of the monodisperse aerosol samples tested agreed within 5% of each other, whereas 40% of the samples agreed within 5% for the polydisperse aerosol. The difference is attributed to finite binning, and the resulting lower bin counts, which deteriorate counting statistics in both spectrometers, leading to higher uncertainty. The measured relative bias for particle size measurement of PAMS is within the 25% accuracy limit recommended by NIOSH for the direct-reading instruments (NIOSH 2012). It should be noted that this size measurement (or sizing) accuracy (given by the bias, b) is not the same as the accuracy of measurement of the number-weighted particle size distribution, which also depends on the accuracy of particle number concentration measurement.

The measurement time at each voltage step (t_{step}) can influence the accuracy of measured distribution. If t_{step} is smaller than the time required to reach a steady concentration of the aerosol downstream of the DMA, it will lead to smearing of the measured distribution. On the other hand, larger t_{step} will result in longer measurement times. To ensure steady-state measurements downstream of the DMA, a wait time (t_{wait}) was introduced at each voltage step. The counts measured during this wait

Table 2. Comparison of geometric mean diameter and geometric standard deviation of lognormal fits to measured distributions of near-monodisperse aerosols from PAMS and EMS at (a) high resolution and (b) low resolution.

(a)

Input mono-disperse size, d_{DMA} (nm)	High resolution, $\beta = 0.125$, Preexisting charge = 0				High resolution, $\beta = 0.125$, Preexisting charge = +1			
	PAMS		EMS		PAMS		EMS	
	d_{pg}	σ_g	d_{pg}	σ_g	d_{pg}	σ_g	d_{pg}	σ_g
19	18.9	1.07	18.8	1.06	19.0	1.06	18.7	1.06
32	30.9	1.06	31.5	1.05	30.7	1.07	31.2	1.06
55	50.0	1.07	53.5	1.06	49.8	1.07	53.0	1.06
97	88.0	1.07	93.3	1.06	88.7	1.08	94.8	1.05
150	138.0	1.07	146.8	1.07	142.0	1.08	148.1	1.08
250	230.3	1.08	250.2	1.08	231.0	1.08	244.0	1.08
360	330.9	1.13	364.3	1.10	341.3	1.13	368.2	1.09

(b)

Input mono-disperse size, d_{DMA} (nm)	High resolution, $\beta = 0.125$, Preexisting charge = 0				High resolution, $\beta = 0.125$, Preexisting charge = +1			
	PAMS		EMS		PAMS		EMS	
	d_{pg}	σ_g	d_{pg}	σ_g	d_{pg}	σ_g	d_{pg}	σ_g
19	20.3	1.08	N/A	N/A	20.4	1.09	N/A	N/A
32	32.6	1.09	33.0	1.09	32.1	1.10	32.8	1.09
55	61.2	1.36	60.6	1.12	59.1	1.35	60.4	1.13
97	107.0	1.18	109.0	1.10	108.2	1.12	109.3	1.10
150	131.0	1.17	119.1	1.13	141.3	1.13	126.6	1.15
256	299.0	1.11	301.3	1.11	298.1	1.10	303.1	1.12
372	433.73	1.09	441.5	1.09	436.1	1.09	441.4	1.09

period (i.e., $t = 0$ to t_{wait}) were ignored. Only the counts measured between time t $= t_{wait}$ to t_{step} were used for the size distribution measurement. Figure S9 in the SI shows the effect of wait time (t_{wait}) on the measured distribution of polydisperse aerosols. Variation of the mode or peak diameter (d_{peak}) and the geometric mean diameter (d_{pg}) of the test aerosols is shown. The values of t_{step} below 3 s lead to noticeable bias in the measured peak diameters. Based on these considerations, $t_{step} = 6$ s and $t_{wait} = 3$ s were used in this study.

3.2. Polydisperse aerosols

Table 3 compares size distributions measured from both EMS and PAMS for polydisperse aerosols with N_{tot} ranging from very low (~500 cm^{-3}) to very high (~5 × 10^6 cm^{-3}) in low- and high-resolution modes. The difference in the distributions from two spectrometers was quantified using a mean error (ε_{wm}), defined as

$$\varepsilon_{wm} = \frac{\sum_{i=1}^{M} abs\left(n_{EMS}(d_{p_i}) - n_{PAMS}(d_{p_i})\right)}{\sum_{i=1}^{M} n_{EMS}(d_{p_i})}, \qquad [2]$$

where d_{pi} is the nominal diameter of the ith bin, and $n_{EMS}(d_p)$ and $n_{PAMS}(d_p)$ are size distribution functions for EMS and PAMS, respectively. Table 3 also shows geometric mean and peak diameter, and geometric standard deviation for various aerosol samples measured by the two spectrometers, along with the ε_{wm} . The calculated mean error (ε_{wm}) for high concentration aerosol is about 29.1% (26.3% at high resolution), and increases to 65.7% at low concentrations (N_{tot} ~ 500 cm^{-3}). As will be shown later, this difference in distributions is comparable to that of the other spectrometers.

Figure 3 shows comparison of number-weighted size distributions measured by PAMS to those measured using various commercially available mobility spectrometers including, SMPS (Model 3936 and 3034, TSI, Inc.), WPS (Model 100XP, MSP Corp., Shoreview, MN, USA), and NanoScan (Model 3910, TSI Inc.). Specific charger configuration, calibration dates, and operating aerosol and sheath flow ratios for the commercial spectrometers are listed in Table S2 in the SI. The test aerosol used for this comparison study was polydisperse ammonium sulfate aerosol generated by pneumatic atomization. The bipolar charger was not used in these experiments; therefore, the test aerosol entering the mobility spectrometers retained its native charge. The inverted size

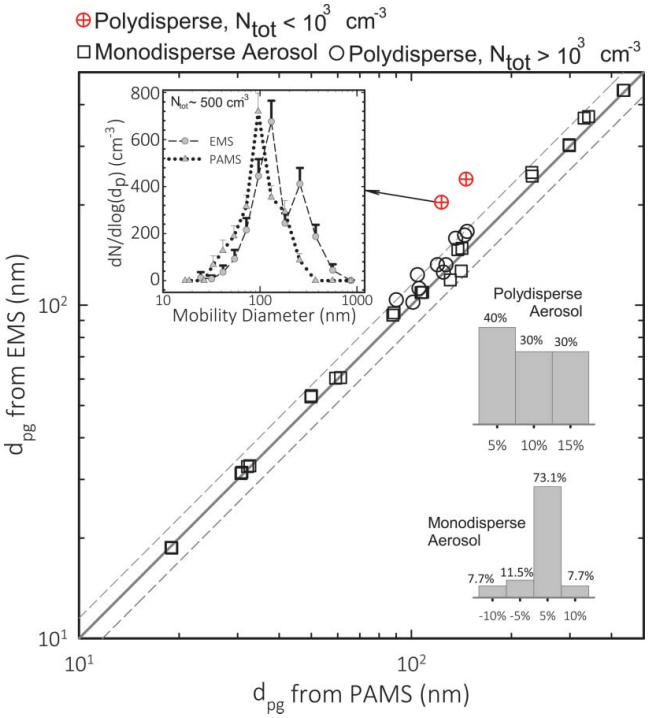

Figure 2. Comparison of sizing accuracy of PAMS and EMS at identical mobility resolution for near-monodisperse and polydisperse aerosols. The inset histograms show percent of samples tested (on the *y*-axis), for each monodisperse and polydisperse aerosol, as a function of percent difference in measured d_{pg} from the two instruments (i.e., $(d_{pg}^{EMS} - d_{pg}^{PAMS})/d_{pg}^{EMS}$).

distributions for each spectrometer were obtained using its commercial inversion software. The comparison in Figure 3 shows that there is general qualitative agreement in the features of the size distributions. The figure also shows mean weighted error ε_{wm}, which was computed using Equation (2). For these calculations, $n_{EMS}(d_p)$ and $n_{PAMS}(d_p)$ in Equation (2) represented the number size distribution of the commercial spectrometer, and that of the PAMS, respectively. Since each spectrometer had a different number of size bins, the distribution was re-binned (using a linear interpolation between the bins) to match the binning of PAMS. The mean weighted error ε_{wm} quantifies the difference between distributions and ranged from 3% to 163%, with no clear trend. Peak and geometric mean diameters generally agree. However, $\frac{dN}{dLogD_p}$ varied substantially across instruments. This difference in $\frac{dN}{dLogD_p}$ could be attributed to several factors including drift in the calibration of the CPCs used in these spectrometers, different calibration techniques used, differences in charging techniques and charger performance, and difference in the inversion algorithms. The $\frac{dN}{dLogD_p}$ measured by the WPS were low, perhaps due to inadequate neutralization in a Po-210 charger. The agreement between the distribution measured by NanoScan and that from other instruments was poor for 250 nm particles (Figure 3b). We surmise that this was likely due to the combination of unipolar charging and low resolution of the classifier. The drastically different distribution measured by NanoScan in Figure 3d was perhaps due to the high preexisting charge on the sampled aerosol. Since NanoScan uses a unipolar charger, high preexisting charge on the particles can lead to higher degree of bias in the measured distributions. This is consistent with previous studies, which have shown that unipolar chargers can lead to large uncertainties when used for mobility size distribution measurements (Qi and Kulkarni 2012; Levin et al. 2015). The instrument comparison in Figure 3 serves to demonstrate the range of deviation (from each other) of measured size distributions across different commercial spectrometers. The overall differences could be attributed to the intrinsic differences in charging, classification, counting, and proprietary inversion algorithms used by various spectrometers.

3.3. Counting statistics

In addition to mobility resolution, another key source of uncertainty of size distribution measurement is the Poisson uncertainty. Relative uncertainty

Table 3. Comparison of size distribution parameters measured by both EMS and PAMS (at $\beta = 0.125$ and 0.25) for aerosols with low (N_{tot} ~ 500 cm^{-3}) to high (~ 5×10^6 cm^{-3}) total number concentration.

	Low resolution, $\beta = 0.25$								High resolution, $\beta = 0.125$						
	PAMS			EMS					PAMS			EMS			
N_{tot} (cm^{-3})	d_{peak}	d_{pg}	σ_g	d_{peak}	d_{pg}	σ_g	% ε_{wm}	N_{tot} (cm^{-3})	d_{peak}	d_{pg}	σ_g	d_{peak}	d_{pg}	σ_g	% ε_{wm}
5.6×10^6	59.7	90.1	1.9	73.3	103.7	1.8	29.1	5.6×10^6	68.0	101.1	1.8	74.1	102.0	1.8	26.3
1.6×10^6	74.7	105.5	1.8	78.1	112.3	1.8	13.7	9.3×10^5	68.9	104.3	1.8	85.0	123.4	1.8	27.2
1.25×10^5	94.5	135.9	1.8	111.9	158.7	1.8	22.4	1.5×10^5	102.8	147.2	1.8	118.1	166.4	1.8	19.8
3.6×10^4	89.8	127.1	1.8	112.0	132.2	1.5	42	4.3×10^4	99.8	144.6	1.8	118.0	162.3	1.8	26.3
3.5×10^3	89.8	119.8	1.8	108.9	132.2	1.5	40.1	3.5×10^3	87.7	124.9	1.5	105.8	125.6	1.5	41.4
5.1×10^2	101.7	123.2	1.6	144.3	203.6	1.8	65.7	1.1×10^3	116.3	146.1	1.8	172.2	238.9	1.8	64.8

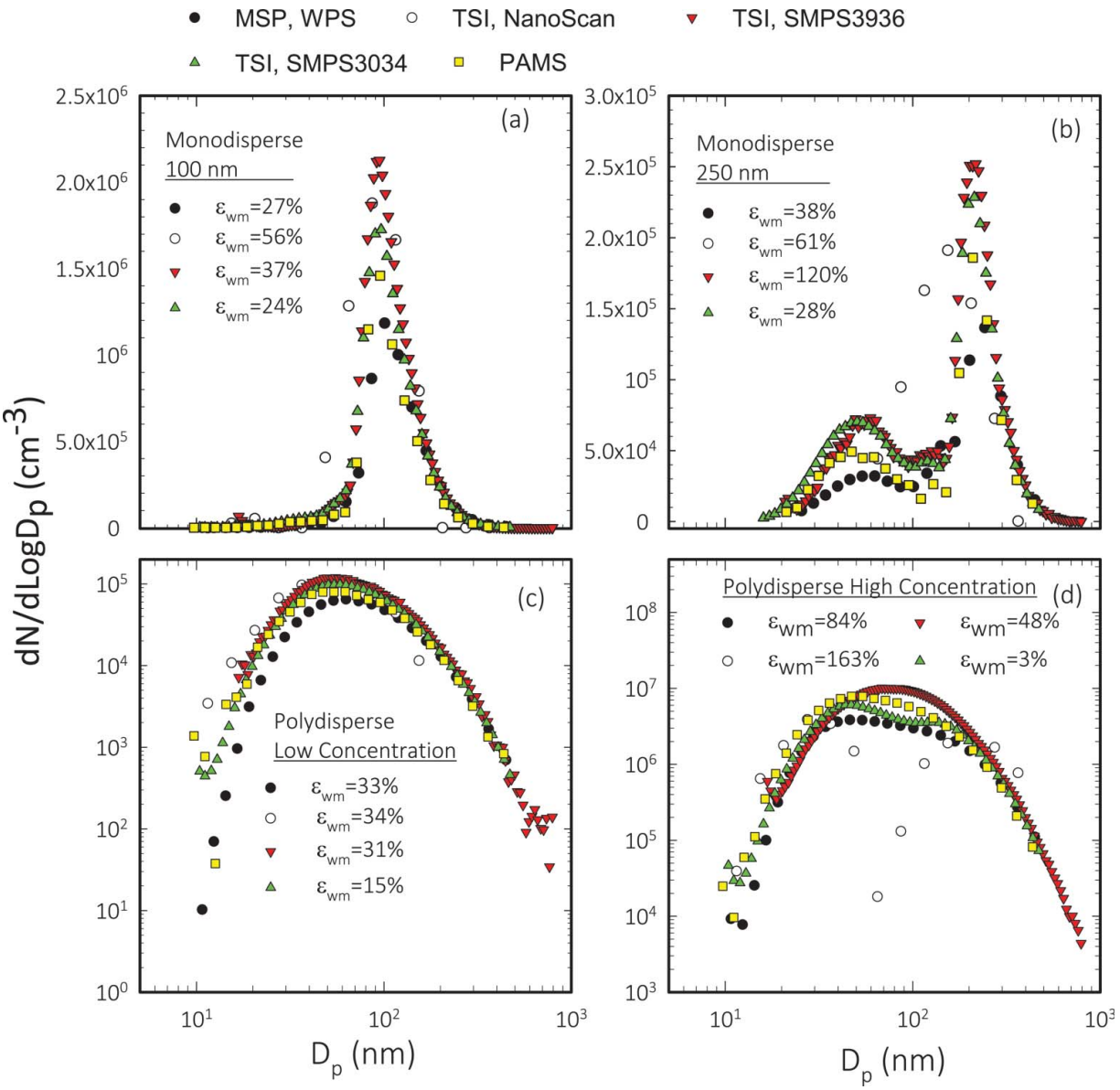

Figure 3. Comparison of particle size distributions of monodisperse and polydisperse aerosol obtained from PAMS with that from various commercial spectrometers. ε_{wm} was computed using Equation (2).

of particle counting events is governed by the Poisson distribution, and is given by $\sqrt{C}/C$ (where C is the total count). Figures 4a and b show estimated percent relative Poisson uncertainty as a function of particle diameter measured by PAMS (a) and EMS (b) using design operating conditions in these instruments. The Poisson uncertainty was theoretically estimated by calculating the detector response (i.e., counts by the CPC) for a given inlet aerosol size distribution, after accounting for charging efficiency, diffusion, transport losses, the DMA transfer function, and the counting efficiency of the CPC. Also shown are two particle size distributions, one measured at a workplace that manufactures carbon nanofibers (CNF; $N_{tot} \sim 10^6$ cm^{-3}; Evans et al. 2010) and an indoor air measured in our laboratory ($N_{tot} \sim 10^3$ cm^{-3}). The estimated Poisson uncertainties of PAMS for measurement of CNF are less than 5% using PAMS; whereas those for the indoor laboratory air are around 50% at 15 nm and increase to 200% for larger diameters around 855 nm. This is due to relatively low counts of larger particles in the size distribution. Figure 4b shows similar data for EMS (consisting of TSI 3081 DMA and the ultrafine condensation particle counter, TSI 3776 or 3025). This combination of DMA and the CPC has been widely used for size distribution measurements. The EMS was operated at typical flow rates (aerosol flow = 0.3 L/min, sheath flow = 3 L/min), and in stepping mode with identical time steps as in PAMS. The corresponding Poisson uncertainties for EMS were estimated to

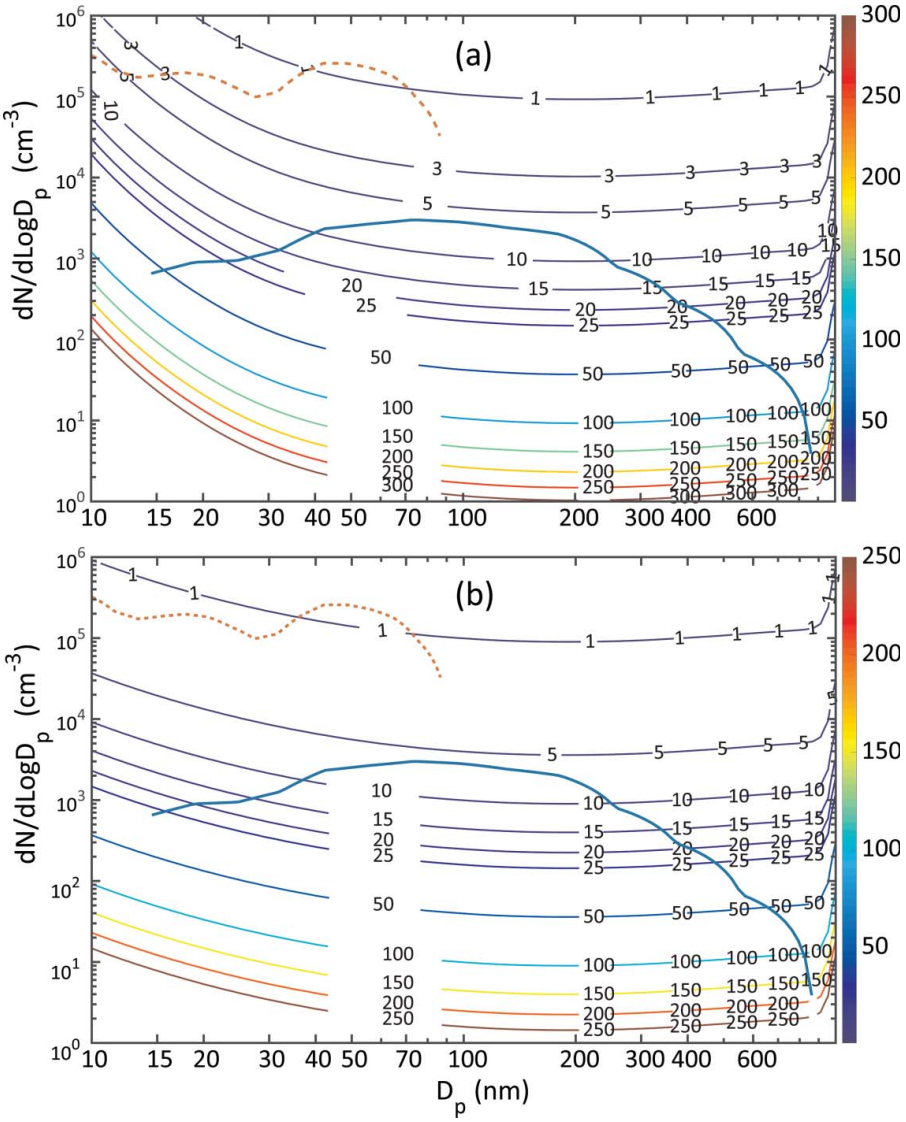

Figure 4. Contour map showing theoretically estimated Poisson uncertainty for (a) PAMS and (b) EMS using CPC 3776 (or 3025) at different number concentration levels (on the *y*-axis) and particle sizes (on the *x*-axis) of the sampled aerosol. The contour lines showing relative percent uncertainty are color coded (red: high, blue: low; the contour labels show the numerical value of relative percent uncertainty). Also shown are two particle size distributions of aerosol, one measured at a carbon nanofiber manufacturing facility (brown, dotted line), and the other in a clean indoor laboratory (blue, solid line). The plots allow assessing counting uncertainty of measurement at a given $dN/d\text{Log}d_p$ and d_p of the sampled aerosol. The counting uncertainties of PAMS at very low number concentrations can be high; however, they are comparable to those of widely used mobility spectrometer configurations employing the CPC 3776 or CPC 3025.

be about 30% at 15 nm and 180% at 872 nm. This comparison shows that though the counting statistics of PAMS can be poor for very dilute aerosol, the magnitude of this uncertainty is comparable to those from the commonly used mobility spectrometer configurations for aerosol measurement.

3.4. Field measurements

Figure 5 shows time series comparison of particle distribution measurements obtained from (a) PAMS and (b) SMPS (TSI Inc., model 3936) for combustion aerosol. Time is plotted on the *x*-axis, the particle diameter on the *y*-axis, and the color coding indicates the magnitude of $\frac{dN}{dLogD_p}$. The PAMS was operated in stepping mode, whereas the SMPS was operated in scanning mode using the manufacturer's inversion routine. The overall measurement time for one distribution was set at 150 s for each instrument. The two instruments sampled combustion aerosol from a propane flame using a common inlet. The flame was arbitrarily brought in and out of the sampling zone of the common inlet to mimic the transients

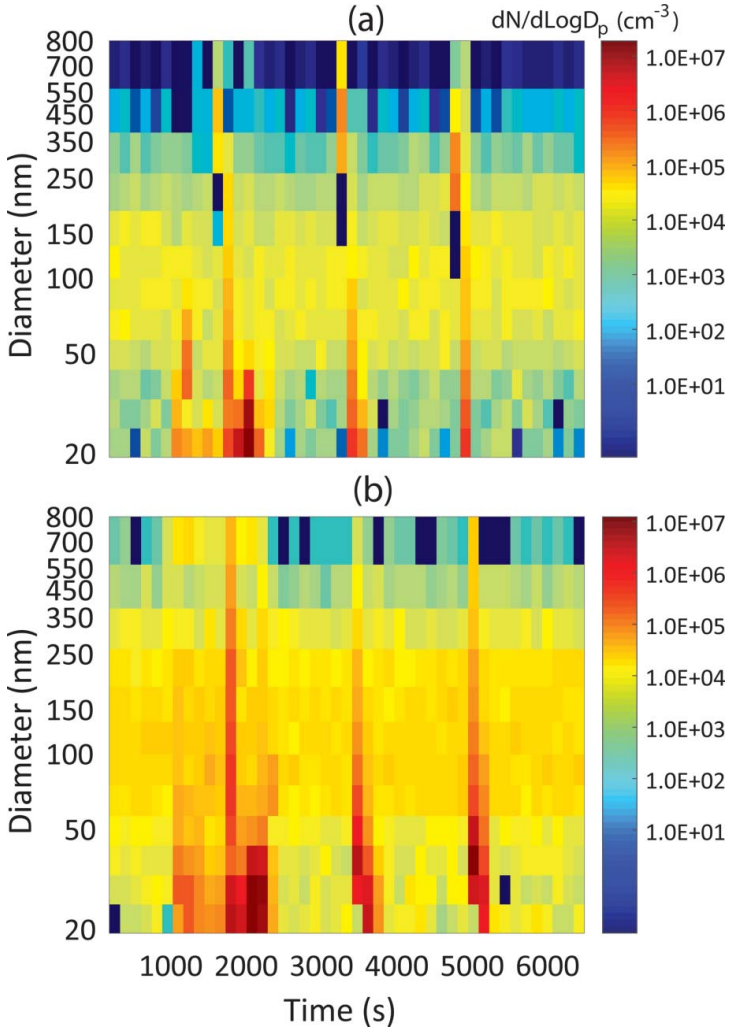

Figure 5. Time series comparison of particle size distribution of (a) PAMS and (b) SMPS™. Combustion aerosol from a propane flame was used as the test aerosol, and was moved in and out of the sampling zone of the two instruments to mimic transient aerosol.

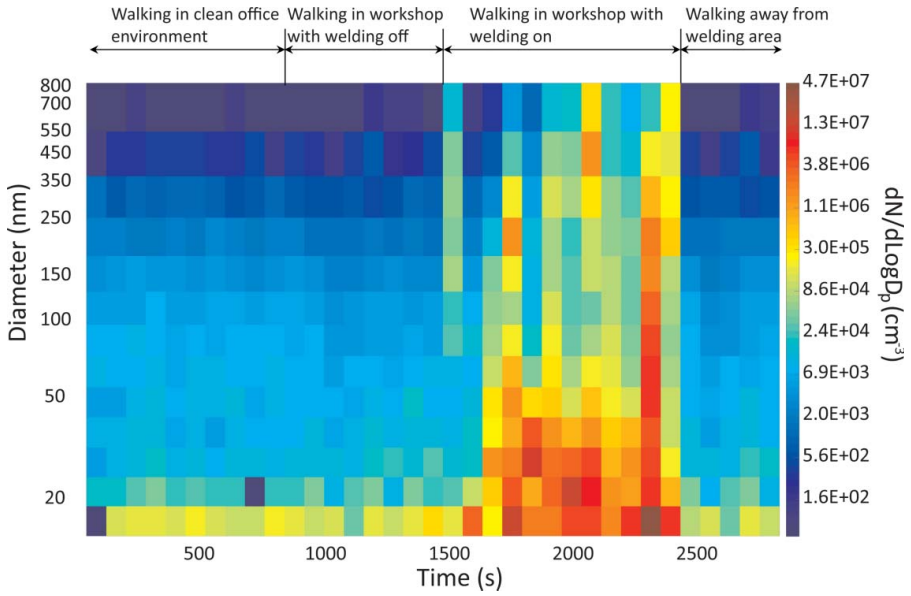

Figure 6. Particle size distribution measured in the breathing zone of a moving person exposed to aerosols emitted by arc welding processes. The instrument prototype was worn by the person, with the inlet of the sampling tube exposed to the breathing zone.

typical in mobile sampling. Figure 5 shows that the key qualitative features of particle size distribution from both instruments compare well. There are differences in $\frac{dN}{dLogD_p}$ in some channels, with PAMS typically reporting lower concentrations, especially at the tail end of the distribution. In addition to different source (and magnitude) of uncertainty in each instrument, some of these difference could be attributed to the different rate at which each instrument steps or scans through the entire distribution (leading to sampling different diameters at different times).

Figure 6 shows time series plot of particle size distribution measured in the breathing zone of a moving person exposed to aerosol emitted by arc welding processes. The instrument prototype was worn by the person, with the sampling inlet tube exposed to the breathing zone. The particle size distributions are continuously measured and recorded by the instrument prototype. Figure 6 shows that the transient exposures in the breathing zone are adequately captured by the instrument. These size distributions can be further used to obtain approximate estimation of mass, surface area, and number concentration of the aerosol. Another example of mobile sampling capability of PAMS is shown in Figure 7, which shows the aerosol concentration of 20 nm diameter particles inside and outside of a N95 respirator worn by a moving person exposed to arc welding aerosol. These data were obtained by using two prototype units worn by the person, one to monitor the inside concentration, and the other to monitor the outside concentration. The measurement capability of the instrument can be used for such on-person or mobile measurements that were previously not possible.

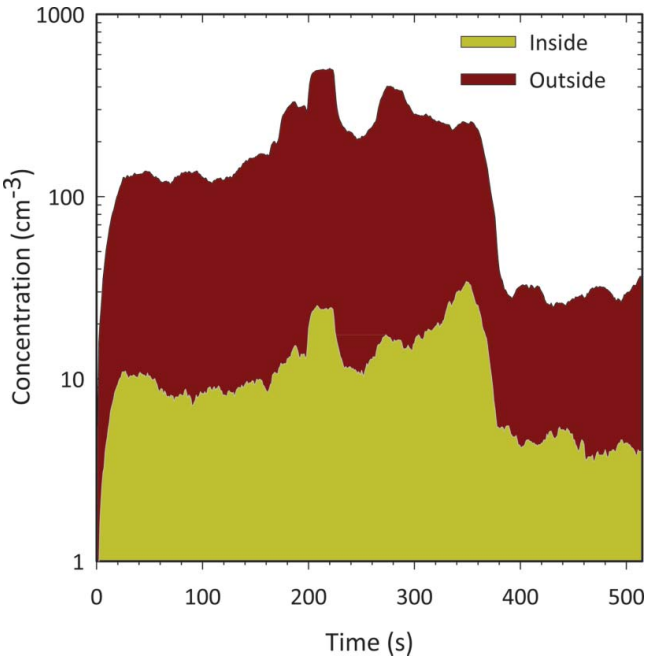

Figure 7. Concentration of 20 nm diameter particles measured simultaneously inside and outside of the respirator worn by a person moving near a welding operation. Two prototype instruments were used on-person to obtain continuous measurement of nanoparticles simultaneously inside and outside the respirator.

4. Conclusions

A portable mobility spectrometer for size distribution measurement of nanoparticles and submicrometer aerosol has been developed. Use of a corona-based bipolar charger allows unrestricted transportation of the instrument and access to sampling sites. The use of bipolar charger in PAMS also permits making measurements over extended size range. However, when using a corona-based charger, frequent cleaning of charger is necessary to ensure reliable measurements. The overall sizing accuracy of PAMS was well within the NIOSH accuracy criteria of 25% for the direct-reading air quality instruments (NIOSH 2012). Comparison with several commercial mobility spectrometers showed that the measured size distributions agree well within the combined uncertainties from charging, sizing, counting, and numerical inversion in these instruments. Proper operation of the condensation particle counter also requires maintaining near-upright orientation, limiting its use to applications where such orientation can be maintained. PAMS offers several unique advantages with respect to existing commercial hand-portable mobility spectrometers: (i) much smaller size and weight, (ii) better measurement precision due to the use of bipolar charger, and (iii) ability to measure wider particle size range below 1 micrometer. These attributes make PAMS well-suited for nanoparticle and submicrometer aerosol exposure measurements and other mobile aerosol sampling applications.

Nomenclature

b	relative bias defined as $\frac{d_{pg}-d_{DMA}}{d_{pg}}$
C	total particle count by CPC or detector
D_p *or* d_p	particle diameter
d_{pg}	geometric mean diameter of the number-weighted particle size distribution measured by the mobility spectrometer
d_{DMA}	centroid diameter of the aerosol classified by the classifying DMA used to produce calibration aerosol
d_{50}	diameter of the particle activated with 50% detection efficiency in CPC

d_{pi}	nominal central channel/bin diameter of ith bin in PAMS or EMS
d_{peak}	peak or mode diameter of the number-weighted size distribution
$f_{chg}(i, d_p)$	probability that particle of diameter d_p will carry charge i before entering the DMA classification zone
$n_{EMS}(d_p)$	number-weighted size distribution function measured by EMS
$n_{PAMS}(d_p)$	number-weighted size distribution function measured by PAMS
N	cumulative total number concentration in a size distribution function $\frac{dN}{d\mathrm{Log}D_p}$ or $\frac{dN}{d\mathrm{Log}d_p}$
N_{tot}	size-integrated total number concentration of aerosol
N_i	number concentration of aerosol downstream of mDMA corresponding to voltage V_i
Δt	temperature differential between and hot and cold sections of the CPC
t_{wait}	wait time at each voltage step V_i in PAMS, before starting recording of number count by CPC
t_{step}	time for which the voltage V_i is applied at step i.
V_i	voltage on central electrode of mDMA corresponding to step i

Greek symbols

β	ratio of aerosol flow to sheath flow (volumetric) in mDMA
ε_{wm}	mean error defined by Equation (2); denotes relative difference between two measured distributions.
$\eta_{tot}(d_p)$	total size-dependent particle detection efficiency
η_{diff}	diffusional wall losses in the transport lines
η_{cycl}	transmission efficiency of the inlet cyclone
η_{chg}	transmission efficiency of the bipolar charger
η_{det}	detection efficiency of the CPC
$\Omega(V_j, i, d_p)$	transfer function of the mDMA corresponding to voltage V_j for particle with diameter d_p and charge i

Acknowledgments

Support from engineers at Kanomax Japan Inc. for their help with construction of prototype instrument is gratefully acknowledged. The authors would like to thank Gregory Deye and Liming Lo of NIOSH for helpful comments on the manuscript. Comments from anonymous reviewers are also gratefully acknowledged. The findings and conclusions in this report are those of the authors and do not necessarily represent the views of the National Institute for Occupational Safety and Health. Mention of product or company name does not constitute endorsement by the Centers for Disease Control and Prevention.

References

Birch, M. E., Ku, B.-K., Evans, D. E., and Ruda-Eberenz, T. A. (2011). Exposure and Emissions Monitoring During Carbon Nanofiber Production-Part I: Elemental Carbon and Iron-Soot Aerosols. *Ann. Occup. Hyg.*, 55:1016–1036.

Chen, D. R., and Pui, D. Y. H. (1997). Numerical Modeling of the Performance of Differential Mobility Analyzers for Nanometer Aerosol Measurements. *J. Aerosol Sci.*, 28:985–1004.

Dahm, M. M., Evans, D. E., Schubauer-Berigan, M. K., Birch, M. E., and Fernback, J. E. (2012). Occupational Exposure Assessment in Carbon Nanotube and Nanofiber Primary and Secondary Manufacturers. *Ann. Occup. Hyg.*, 56:542–556.

Evans, D. E., Ku, B. K., Birch, M. E., and Dunn, K. H. (2010). Aerosol Monitoring During Carbon Nanofiber Production: Mobile Direct-Reading Sampling. *Ann. Occup. Hyg.*, 54:514–531.

He, M., and Dhaniyala, S. (2013). A Multiple Charging Correction Algorithm for Scanning Electrical Mobility Spectrometer Data. *J. Aerosol Sci.*, 61:13–26.

Hoppel, W. A. (1978). Determination of the Aerosol Size Distribution from the Mobility Distribution of the Charged Fraction of Aerosols. *J. Aerosol Sci.*, 9:41–54.

Levin, M., Gudmundsson, A., Pagels, J. H., Fierz, M., Mølhave, K., Löndahl, J., Jensen, K. A., and Koponen, I. K. (2015). Limitations in the Use of Unipolar Charging for Electrical Mobility Sizing Instruments: A Study of the Fast Mobility Particle Sizer. *Aerosol Sci. Technol.*, 49:556–565.

Methner, M., Hodson, L., and Geraci, C. (2010). Nanoparticle Emission Assessment Technique (Neat) for the Identification and Measurement of Potential Inhalation Exposure to Engineered Nanomaterials—Part A. *J. Occup. Environ. Hyg.*, 7:127–132.

NIOSH (2012). *Components for Evaluation of Direct-Reading Monitors for Gases and Vapors*. US DHHS, Washington, DC.

NIOSH (2013). *Current Intelligence Bulletin 65: Occupational Exposure to Carbon Nanotubes and Nanofibers*. National Institute for Occupational Safety and Health, Cincinnati, OH.

Qi, C., Asbach, C., Shin,W. G., Fissan, H., and Pui, D. Y. H. (2009). The Effect of Particle Pre-Existing Charge on Unipolar Charging and Its Implication on Electrical Aerosol Measurements. *Aerosol Sci. Technol.*, 43:232–240.

Qi, C., and Kulkarni, P. (2012). Unipolar Charging Based, Hand-Held Mobility Spectrometer for Aerosol Size Distribution Measurement. *J. Aerosol Sci.*, 49:32–47.

Qi, C., and Kulkarni, P. (2013). Miniature Dual-Corona Ionizer for Bipolar Charging of Aerosol. *Aerosol Sci. Technol.*, 47:81–92.

Qi, C., and Kulkarni, P. (2016). Miniature Differential Mobility Analyzer for Compact Field-Portable Spectrometers. *Aerosol Sci. Technol.* DOI: 10.1080/02786826.2016.1221500.

Ramachandran, G., Ostraat, M., Evans, D. E., Methner, M. M., O'Shaughnessy, P., D'Arcy, J., Geraci, C. L., Stevenson, E., Maynard, A., and Rickabaugh, K. (2011). A Strategy for Assessing Workplace Exposures to Nanomaterials. *J. Occup. Environ. Hyg.*, 8:673–685.

Stolzenburg, M. R. (1988). *An Ultrafine Aerosol Size Distribution Measuring System*. Department of Mechanical Engineering, University of Minnesota, St. Paul, Minnesota.

Wiedensohler, A. (1988). An Approximation of the Bipolar Charge Distribution for Particles in the Submicron Range. *J. Aerosol Sci.*, 19:387–390.